Loughborough University

This item was submitted to Loughborough's Institutional Repository (https://dspace.lboro.ac.uk/) by the author and is made available under the following Creative Commons Licence conditions.

For the full text of this licence, please go to:
http://creativecommons.org/licenses/by-nc-nd/2.5/

Diffusivity variation in Electromigration failure

V.M. Dwyer

School of Electronic, Electrical and Systems Engineering
Loughborough University,
Loughborough, LE11 3JP, UK.
e-mail: v.m.dwyer@lboro.ac.uk

Abstract

Electromigration driven void dynamics plays an important role in the reliability of copper interconnects; a proper understanding of which is made more difficult due to local variations in line microstructure. In simulations, the parameter which best incorporates these variations is the effective atomic diffusivity D_{eff} which is sensitive to grain size and orientation, interface layer thickness, etc. We examine a number of experimental results and conclude that, to explain observations using current theoretical models, D_{eff} values must vary significantly along the interconnect, and that such variations are enough to yield encouraging simulations of resistance variations under bidirectional stress.

1. Introduction

The aggressive scaling of (VLSI) circuits over recent years continually pushes back a complete solution to the problem of Electromigration (EM) induced metallisation failure. With each new technology node, the current density j increases; causing the metal drift velocity v_d to increase and reducing the interconnect lifetime t_f as a result. The link between t_f and j is embodied in the well-known Black equation [1]. However at the 65 nm node and beyond, reductions in lifetime are observed even at the same current density [2]. This has been associated with the coincident change in line microstructure from being primarily bamboo to being primarily a bamboo–polycrystalline mixture containing significant small grain agglomerates [2]. Additional atomic diffusion is thus made possible along the grain boundary networks which make up the polycrystalline regions [2]. The metal drift velocity is determined by a balance between the EM force term, proportional to j, and the back-stress force proportional to the gradient in the tensile stress σ[3]. As v_d is proportional to the atomic mobility and consequently also, through the Einstein relation, to the atomic diffusivity, the opening of new diffusion paths causes its increase. The link to the failure time t_f ultimately relies on the assumed continuity relation.

A great deal of attention has been paid to the quality of the copper/cap-layer interface (particularly through the introduction of metal caps such as CoWP [4]) as this interface has represented the dominant metal migration path in recent years. At the 65 nm node however, the change in the line microstructure to a bamboo–polycrystalline mix necessarily creates an atomic diffusivity which varies with position along the line.

A strong (111) texture has long been felt important to increasing interconnect lifetime [5], as has the number of higher mobility, high-angle grain boundaries (HAGBs), e.g. [6]. Such properties vary on the scale of the grain size. Failure locations are also often associated with the occurrence of grain boundary grooving and the presence of grain boundary triple points. Pipe diffusion along dislocations of total cross section $a_{pipe}(x)$, at position x along the line, may prove to be an important contributor particularly if the metal is under stress close to its elastic–plastic transition [7]. A number of these issues may also prove important in the understanding of EM failure under bidirectional current stress, as cycling through a sequence of voiding, void growth and void filling/healing may affect the microstructure at the line ends.

Crudely these effects may be included in a local diffusivity value which, ignoring the slower bulk diffusion, may be written as

$$D_{eff}(x) = \frac{\delta_I(x)}{h} D_I(x) + \frac{\delta_{GB}}{d(x)} D_{GB}(x) + \frac{a_{pipe}(x)}{hw} D_{pipe}(x) \quad (1)$$

which is an averaged value over the line cross–section $h \times w$. In polycrystalline regions, where the grain size $d(x)$ is relatively small, grain boundary diffusion will play a more important role.

The velocity of a drifting void appears to be determined by the crystal orientation of the grain over which it drifts and it is to be expected that the atomic cap–layer interface diffusivity D_I, will vary with crystallographic orientation in a similar manner, particularly in bamboo regions. The interfacial adhesion is likely to have an impact on the interface effective thickness δ_I, and consequently it too may vary along the line length. In general the impact of HAGBs and other

effects will contribute to a position dependent D_{eff}. Such local variations in drift velocity can cause the atomic/vacancy traffic to jam at points other than the cathode via, thus complicating any analysis.

For now, it seems a reasonable approximation to assume that D_{eff} will vary along the line length in a roughly piecewise–constant fashion, Fig. 1. To simplify matters we shall model the lengths of polycrystalline sections as deriving from the same distribution as the bamboo grains. As a consequence, the lengths d_k of constant diffusivity are chosen from a lognormal distribution and the effective diffusivities $D_{eff,k}$ from a lognormal mixture with a mixture fraction p representing the fraction of slow diffusion sections.
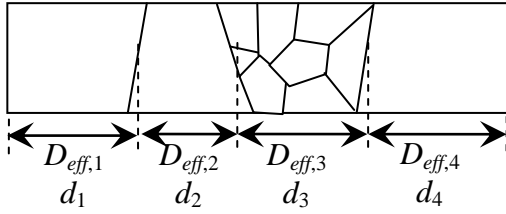

Figure 1. A schematic microstructure made from a polycrystalline–bamboo mixture. This may equally be a top view or a side view of the interconnect.

In addition to the extra lifetime reduction at the 65 nm node, there are a number of other microstructure related issues which have been associated with Electromigration failure. For example, it has been observed that voids can nucleate at inline points (usually pinned to grain boundaries (GBs)), [8, 9]. In such cases, the grain at the cathode–most end of an inline void tends to possess a (111) out of plane orientation, or a close relation, while the orientation of the anode–most grain tends to be either from a different family or to be a more distant (111) relative [8, 9]. In some cases these voids grow and de–pin from the GB, while others shrink and heal [8, 9]. Voids that have de-pined, and drift along the cap–layer interface do so at a rate determined by the orientation of the crystals they drift over [8]. Such affects appear to be due to the presence of atomic flux divergences created by the discontinuities in the effective diffusivity $D_{eff,k}$. Naturally, as the diffusivity values determine the rates of stress build up and void growth, a distribution of diffusivity values $f_D(D_{eff})$ will lead to a distribution of failure times, all other things being equal. Consequently $f_D(D_{eff})$ will account for some portion of the lognormal standard deviation observed in virtually all failure time distributions [10]. We shall show that, in order to simulate such void nucleation and void dynamics, a broad distribution $f_D(D_{eff})$ is required. It is fairly clear that the blocking of the vacancy flux sufficiently to allow a void to nucleate inline is likely to require an effective diffusivity substantially smaller than the average.

This raises a number of important questions. What kinds of distributions $f_D(D_{eff})$ are consistent with the experimental observations? What implications do such broad distributions have for other aspects of EM failure?

In the general description of EM failure, a consideration of inhomogeneous diffusivity effects is undertaken only when necessary. Nucleation of inline voids and the detachment of voids from GBs will require such interventions. With the bamboo/polycrystalline mix and the importance of void dynamics the simple, homogeneous view probably needs now to be revisited.

2. The model

The Stress Evolution Module (SEM) of Korhonen et al. [3] has proved to be very useful in describing EM effects. It describes the developing tensile stress $\sigma(x,t)$ under the combined EM and back–stress forces as

$$J = \frac{D_{eff}(x)}{k_B T}\left(\frac{\partial \sigma}{\partial x} - \frac{Z^*q\rho j}{\Omega}\right), \qquad \frac{\partial \sigma}{\partial t} + B\Omega \frac{\partial J}{\partial x} = 0 \quad (2)$$

where J is the atomic flux ($= v_d/\Omega$), and $D_{eff}(x)$ is the piecewise constant effective atom diffusivity averaged over the line cross–section. B is the bulk modulus, Ω is the atomic volume, $k_B T$ is the thermal energy Z^*q is the effective copper charge and $E = \rho j$ is the electric field within the metal. As in ref. [10] this is converted into a finite element expression based on chapeau shape functions and a mesh X_k ($k=1,2,\ldots,N+1$) consisting of the set of grain boundary points chosen according to some distribution $f_d(d)$, with median size d_{50}, and superimposed on a regular mesh of size $d_{50}/5$, [12]. Here the grain size distribution is taken to be lognormal with $d_{50} = 0.25$ μm and a lognormal variance of $\sigma_d = 0.3$, Fig. 1. The dimensionless variables, $X = x/\ell$ (in terms of length scale ℓ chosen to be 2 μm, as a midrange value between a typical median grain size d_{50} and a typical line length L), $\tau = D_{ref}t/\ell^2$ (for characteristic effective diffusivity D_{ref}) and

$$c_k = \frac{\Omega \sigma(x_k,t)}{k_B T}, b = \frac{B\Omega}{k_B T}, \chi = b\frac{\Omega J \ell}{D_{ref}},$$

$$\alpha = \frac{Z^*q\rho j}{k_B T}\ell, \kappa_{effk} = \frac{bD_{eff,k}}{D_{ref}}$$

turn eqns (2) into the finite element set (ref. [10])

$$\boldsymbol{M}\frac{d\boldsymbol{c}(\tau)}{d\tau} = -\boldsymbol{K}\boldsymbol{c}(\tau) + \alpha\begin{bmatrix}0\\\boldsymbol{\kappa}\end{bmatrix} - \alpha\begin{bmatrix}\boldsymbol{\kappa}\\0\end{bmatrix} + \begin{bmatrix}\chi(0,\tau)\\\boldsymbol{0}\\-\chi(L,\tau)\end{bmatrix} \quad (3)$$

The tridiagonal matrices $\boldsymbol{M}$ and $\boldsymbol{K}$ respectively depend upon mesh sizes $\varepsilon_k = X_k - X_{k-1}$ and κ/ε values and $\boldsymbol{\kappa}$ is the vector of normalized effective diffusivities κ_k. Values for the physical parameters in eqn (3) are as given in ref. [10].

Eqn (3) may be used to investigate the nucleation, growth and shrinkage of voids (e.g. in the case of bidirectional stress), at both inline points or at the cathode via. If a void forms at the cathode, at $X = L$ say, then the increase in normalized void length (volume $= hw\ell L_{void}(\tau)$) due to the current $\chi(L,\tau)$ is

$$L_{void}(\tau) = \frac{1}{b}\int_0^\tau \chi(L,\tau')d\tau' \quad (4)$$

2

For a unidirectional current stress over the interval $(0, \tau)$

$$c(\tau) = c(\infty) + \exp(-Q\tau)(c(0) - c(\infty)) \qquad (5)$$

where $Q = M^{-1}K$, $c(0)$ is the initial (including thermal) stress and the asymptotic ($\tau \to \infty$) stress is given by

$$c(\infty) = \alpha K^{-1}\left(\begin{bmatrix} 0 \\ \kappa \end{bmatrix} - \begin{bmatrix} \kappa \\ 0 \end{bmatrix}\right) \qquad (6)$$

If the associated stress σ is less than the nucleation stress σ_{cr} it is unlikely that a void will form; this corresponds to a length condition of $L < L_{cr}$ where L_{cr} is related to σ_{cr}.

3. Inline void growth

Both Hauschildt et al. [11] and Choi et al. [8, 9] have used the growth rate of inline voids, pinned at grain boundaries, to determine the variation in interfacial diffusivity values. Both obtain a value of around $r = 0.25$ for the ratio of slowest to fastest diffusivity values. Choi et al. [13] argue that, as this value is insufficient for EM nucleation of inline voids, so such voids must necessarily have pre–existed. However, while $r = 0.25$ is indeed insufficient to allow for inline nucleation, it also seems insufficient to describe any of the other texture related issues surrounding EM failure.

As a void nucleates in a homogeneous line, the tensile stress is confined to a region of length $L_{cr}/2$ from the cathode via. The growth of the void to failure, either at the cathode, or pinned to a GB at an inline point, and assuming a critical void volume for failure of V_{cr}, leads to a failure time t_f given by [e.g. 10]

$$\frac{V_{cr}}{\Omega wh} = \int_0^{t_f} \Delta J_{void}(t)dt = \int_0^{t_f} (J_+(t) - J_-(t))dt \qquad (7)$$

where $\Delta J_{void}(t)$ is the net flux of atoms out of the void averaged over the line cross section $h \times w$; and equal to the atomic flux out $J_+(t)$ minus the flux in $J_-(t)$. For a cathode void, $\Delta J_{void}(t) = J_+(t) - 0$, while for an inline void $\Delta J_{void}(t) = J_+(t) - J_-(t)$. In the latter case, $J_-(t)$ is the atomic flux from the cathode into the void. Clearly, all things being equal, cathode voids will grow more quickly than inline voids due to the absence of the draining flux $J_-(t)$. However if the inline void is sufficiently close to the cathode (within the distance $L_{cr}/2$) two new features occur. First the cathode will not itself also be able to void as the stress cannot reach the critical value due to the pinning action of the inline void; and second the back-stress force in the void-cathode region can reduce, and ultimately cut-off, the atomic flux $J_-(t)$. As a consequence both an inline void close to the cathode, and a void at the cathode will, for larger times, grow at similar rates, Fig. 2. For this reason it is unlikely that consideration of the growth of a void pinned to a GB, but close to the cathode, will give much information on the effective diffusivity values.

Fig. 2 shows void growth simulations obtained from solving eqn (3). The dot–dashed curve describes the growth of a cathode void in a 100 μm line while the solid

curve describes the growth of an inline void 10 μm from the cathode. To illustrate our point, we take an extreme example in which, in each case, 90% or the grains are fast diffusing ($p = 0.1$), drawn from a lognormal distribution with a median diffusivity of D_{50fast} and the remaining 10% grains are drawn from a lognormal distribution of median $D_{50slow} = 0.01 D_{50fast}$. Each distribution (fast and slow) has a lognormal standard deviation of $\sigma_D = 0.6$.

If one assumes, as in [8, 9, 11], that the flux out of the void $J_+(t)$ is proportional to D_{ag} (the diffusivity of the grain on the anode side of the void) and that the flux
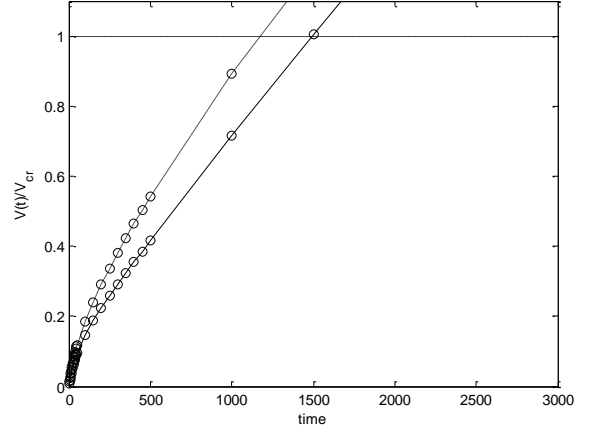

Fig. 2 Void volume growth. Dot–dashed curve is for a void at the cathode and solid curve is of a void 10 μm from the cathode.

into the void $J_-(t)$ is proportional to D_{cg} and that these fluxes are constant in time then eqn (7) implies that the failure time is inversely proportional to $D_{ag} - D_{cg}$. As a result the ratio of failure times for cathode voiding to inline voiding should be $(D_{fast} - D_{slow})/D_{fast}$. From the simulation in Figure 2, one is led to the conclusion that $(D_{fast} - D_{slow})/D_{fast} \sim 1200/1500$, or $r \equiv D_{slow}/D_{fast} = 1/5$. This value is very similar to that obtained from the experimental data in [8, 9, 11], rather than the 'true' value used in the simulation which was r = 0.01. This analysis may also explain why 12–25% of lines in ref. [8] do not fit into the 'slower cathode grain' model, [8]. We conclude that the fluxes $J_+(t)$ and $J_-(t)$ into and out of the void are not only determined by the neighbouring grains, but by something rather more complex. This can also be seen most clearly by considering the steady state flux between two voids or between a pad and a void, where both the end points correspond to regions of stress relaxation (tensile stress $\sigma = 0$). In this case, the steady state flux between the two voids is given by an inverse effective diffusivity D_{eff}^{-1} which is an *average* of all the inverse grain diffusivities $D_{eff,k}^{-1}$ between the voids, weighted by the individual grain sizes [13], rather than simply the neighbouring grains. The reason for this is that faster grains can readily redistribute material, producing a local stress gradient and leading to a reduced atomic flux able to meet those of their slower neighbours.

3

4. Inline void nucleation

For a line with a homogeneous diffusivity, or if the distribution is too narrow, it is not possible to build up tensile stress outside of the region of roughly $L_{cr}/2$ from the line ends. This restriction means that EM can only nucleate inline voids within a distance of, at most, a few tens of microns from the via. Voids found elsewhere must have another origin, including potentially the fabrication process. Even within this region it is difficult to organize conditions under which a void can nucleate. As pointed out in [13], a value of $r \approx 0.25$ is unable to create these conditions, leading to their conclusion that all inline voids necessarily pre-exist. On the other hand if, as above, r is much larger then such voids may result from EM.

The conditions required are, of course, that at a grain boundary, the flux of atoms is effectively blocked. This may be due to a region of correlated slow diffusivities on the cathode most side of the GB and a similar, correlated region of fast diffusivities on the anode most side. Such long range correlations may occur as a result of the fabrication process, as various portions of the chip may be exposed to different fabrication conditions. These possibilities are ignored in the first instance.

Fig. 3 shows the tensile stress near the cathode in a line with a single slow grain, in this case the single rogue slow grain close to the cathode, with $r = 0.01$ (the grain position is indicated by the position of the steep negative gradient in the tensile stress). The various plots show the normalized stress profile σ/σ_{cr} at different positions of the slow grain up to 25 μm from the cathode in a 200 μm line. Further than around 20 μm from the cathode the void nucleates at the cathode, while closer than that the void nucleates at the slow grain.
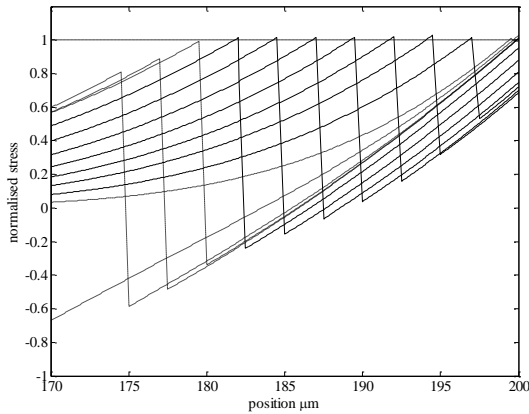

Figure 3. Stress (normalised to critical nucleation stress). Dot – dashed lines nucleate at the cathode via, solid curve nucleate inline. With r = 0.01 inline voids nucleate ~ 15 μm form the via. Grain size = 0.25 μm.

5. Other texture issues

5.1. The distributed stress.

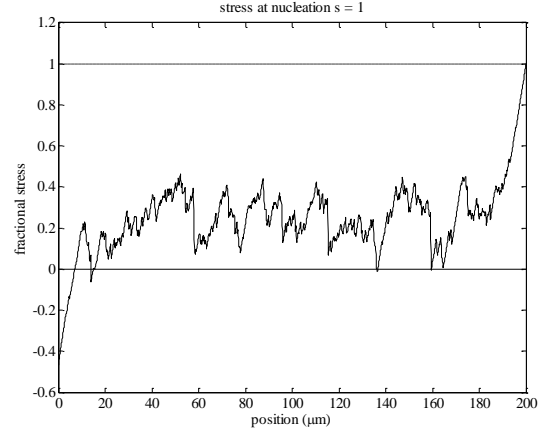For a constant atomic flux to pass through a section of line composed of both fast and slow grains, the faster

Figure 4. Simulated tensile stress as a fraction of that required for nucleation. Here $p = 0.4$, $r = 1/30$ and an initial thermal stress 10 MPa.

grains merely have to redistribute material setting up the local stress gradients to drive $\partial\sigma/\partial x$ closer to $Z^*q\rho j/\Omega$, so offsetting the difference in D_{eff} values. The result is a complex distribution of stress along the line. Commonly stress is assumed to be located only close to line ends. This is valid for homogeneous lines; an example of the current case is shown in Fig.4.

5.2. The effect of line length on σ_t.

It is expected that, as in [14], the mean equivalent homogeneous diffusivity for a line made from a fraction p slow grains and a diffusivity ratio r should be roughly

$$\frac{1}{D_{eff}} = \frac{p}{D_{slow}} + \frac{1-p}{D_{fast}} \Rightarrow D_{eff} \approx \frac{D_{slow}}{p} = \frac{r}{p}D_{fast} \qquad (8)$$

assuming that $D_{fast} >> D_{slow}$. Experiments show that, as the line length L is reduced, the failure time distribution remains lognormal, but with an increased lognormal variance σ_t^2 [15]. This may be partly related to the fact that, for small L, fewer grains are involved in the averaging process leading to greater variation between lines (essentially a less effective Central Limit). Figure 5, shows failure time distributions, with $p = 0.4$ and $r = 0.01$, for lines of lengths $L = 50$ μm and 200 μm.
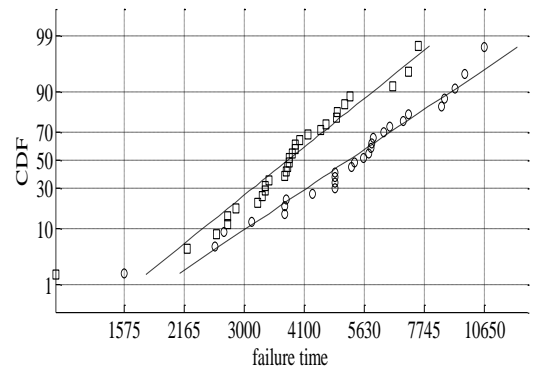

Figure 5. Simulated failure time distribution for $r = 0.01$, a slow fraction of $p = 0.4$ and the lognormal standard deviation, for both fast and slow grains, of 0.6. L=50 μm (marker o) and $L = 200$ μm (marker □).

5.3. The resistance behavior under bidirectional stress.

Recently a number of authors [e.g. 16, 17] have published line resistance plots under periodic bidirectional stress. References [16] and [17] are interesting in particular due to the contrasting test structures used. In [16] a Cu/SiCOH interconnect test structure is used, from a 65 nm CMOS process; single damascene at the lowest metal layer M1 and dual damascene at metal layers M2 and M3. The Cu M2 test line (200μm × 0.3μm) is connected to broader lines (several μm wide) in M1 at one end and in M3 at the other. A schematic of the asymmetric test structure used is shown in Fig. 6. In contrast, in ref. [17], tests are performed in symmetric Dual Damascene structures. Void properties at the two ends are expected to be similar in ref. [17] but might be different in ref. [16].
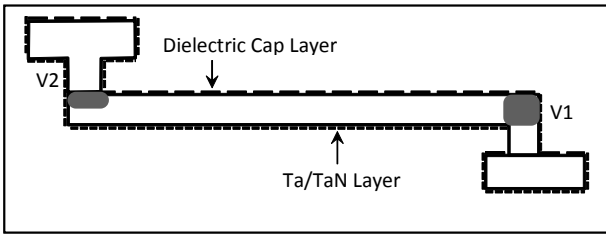

Figure 6. M2 Cu test structure 200 μm × 0.3 μm from ref. [16]. One end is connected to M1 (via below) and other to M3 (via above).

Once a void covers the electron path ($v(t) = v_{cr}$) the shunting through the liner causes a step increase in the line resistance $R(t)$ denoted by R_{step} [17]; $R(t)$ then increases at a constant rate ω (per void volume). Thus the increase in line resistance at time t, for voids of volume $v_0(t)$ and $v_L(t)$ at $x = 0$ and $x = L$ respectively, may be written as

$$\Delta R(t) = \Theta\left(\frac{v_0(t)}{v_{cr0}} - 1\right)\left(R'_{step0} + \omega_0 v_0(t)\right)$$
$$+ \Theta\left(\frac{v_L(t)}{v_{crL}} - 1\right)\left(R'_{stepL} + \omega_L v_L(t)\right) \quad (9)$$

where subscripts refer to voids at $x = 0$ (V2) and $x = L$ (V1), $\Theta(.)$ is the unit step function and e.g. $R'_{step0} = R_{step0} - \omega_0 v_{cr0}$. From the structure shown in Fig. 6 [16] it might be expected that, under downstream electron current stress (i.e. M3→M2→M1), a small slit-like void will nucleates at V2 (via above) at a smaller critical volume than that of the larger void (via below) which will nucleates at V1 under similar upstream electron current conditions (i.e. M1→M2→M3). Once the void reaches the critical size, V2 is likely to have to shunt more current through the liner as when V1 cuts off the current, the last copper path lost borders liner, while for V2 it borders cap layer. For V2 longer paths in liner are likely to be suddenly required. Thus the step increase in line resistance R_{step} at the critical point is likely to be larger for V2. If the slit-like void V2 never heals sufficiently, the resistance of the line will remain high as seen in ref. [16], Figure 2. Because a slit–like void at V2 will grow both vertically and horizontally while a larger V1, spanning the line, grows only

horizontally, it is likely that the rate of change ω of line resistance will also be different for the two voids.

Such a situation may be modeled using eqn (3) in a relatively straight-forward manner. The results shown in Fig. 7 correspond to values of $p = 0.4$ and $r = 1/30$, and reproduce the real behavior observed in [16] quite well. The line cycles through periods of void nucleation at the cathode, followed by growth, and then shrinkage and healing after reversal of the direction of the stress current. In the case shown in Fig. 7 two voids are able to survive, one at either end, as is seen in the experiments [16, 17]. This however involves the additional assumption of an initial (thermal) tensile stress of around 10MPa. To obtain similar behavior in a homogeneous line a diffusivity of $D_{fast}/6$ is required (eqn (8) gives a value of $D_{fast}/7.5$); the overall similarity to the experiments is significantly worse.
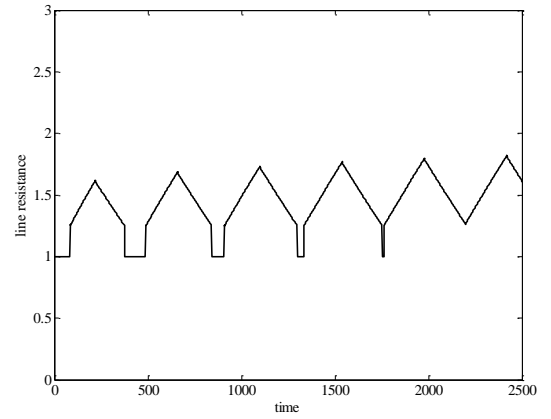

Figure 7. Simulated resistance plot under bidirectional stress. Here $p = 0.4$ and $r = 1/30$. Voids nucleate and grow and heal in a cyclic fashion. Compare with Fig. (3) in ref. [16].
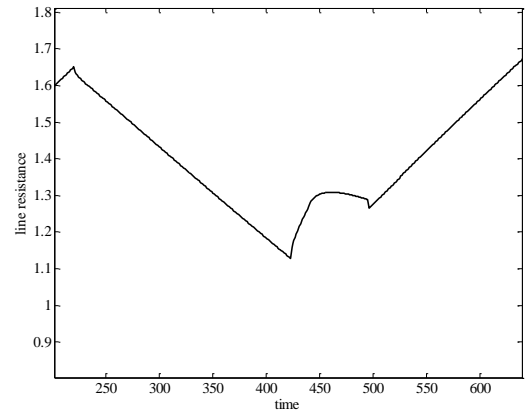
Figure 8. Simulated resistance plot under bidirectional stress. Here p = 0.4 and r = 1/30. Compare with Fig. (2) in ref. [17].

In [17] on the other hand tests were done in Dual Damascene symmetric M3/M2/M3 structure and as a result all via–voids will be of the via–above form, and expected to behave similarly. The same M2 line conditions, and same solution to eqn (3), were used for both Figs. 7 and 8. The differences are only in the critical void volumes, the resistance steps and the growth rates.

5

Values for these are given in arbitrary units in table I. Again the similarity to the experimental results is striking. By comparison, for Fig. 7 see ref. [17, figure 2] and for Fig. 8 see ref. [16, figure 3].

	~[17]	~[16]
R_{step0}	0.025	0.025
ω_0	1.550	0.550
V_{cr0}	0.500	4.000
R_{stepL}	0.025	0.250
ω_L	0.550	0.500
V_{crL}	0.350	3.000

Table I. Parameters used for Figures 7 and 8.

The first column in table I shows the resistance steps R_{step}, resistance slopes ω and critical void volumes V_{cr} used to create Figs. 8. The line here is symmetrical and so the critical volumes and resistance steps are similar. Different resistance slopes were needed to best fit the data, Fig. 2, ref. [17]; this is consistent with the failure analysis conducted afterwards in ref. [17] in which one of the voids was inline whereas the other was at the cathode via, perhaps suggesting grain thinning in one case and edge displacement in the other.

The second column shows the values used to replicate, in Fig. 7, the traces observed in ref. [16, Fig.3]. Growth rates were similar, but resistance steps were very different as a result of the different way, for via–above and via–below, in which the loss of the final path in the copper causes shunting through the liner. Critical values of void size turned out to be similar suggesting that the via–above void V2 was not actually slit–like. This was indeed the case in ref. [16].

6. Conclusions

The extra lifetime reduction at and below the 65 nm node, which is generally associated with microstructural issues, is likely to mean that models of EM failure must include to variation of diffusivity values along the line length. Indeed after ref. [7] it is possible that a time dependence should also be attached to D_{eff}.

As indicated in [13], a value of $r = 0.25$ for the ratio of the slow to the fast diffusivity values is insufficient to explain the nucleation of voids found at inline locations. The authors of ref. [13] conclude the pre-existence of all inline voids while we suggest here that it is the value of $r = 0.25$ that must be reconsidered. We have also analyzed other aspects of EM failure and found that $r = 0.25$ is also incapable of explaining the growth of such inline voids. The upshot of a much larger value of r is that the averaging of the effective diffusivity to allow the assumption of an equivalent homogeneous line, and the resulting conclusion that the stress is concentrated at the line ends, are both likely to be unrealistic.

The impact of a broader distribution of lifetimes, i.e. a larger lognormal standard deviation σ_t of failure times, and the affect of the line length on σ_t are also indicated.

Finally we consider extending the model to a discussion of bidirectional current stressing. Early results from these models show that the line resistance plots obtained experimentally can be reproduced in a relatively straightforward manner. A fuller analysis of these results will be presented elsewhere.

7. References

[1] Black JR, Mass transport of aluminum by momentum exchange with conducting electrons, International Reliability Physics Symposium (Los Angeles, CA, 2011) 148–159.

[2] Hu CK, Gignac L and Rosenberg R, Electromigration of Cu/low dielectric constant interconnects, Microelect. Reliab., **46**, 2006, 213-231.

[3] Korhonen MA, Børgesen P, et al. Stress evolution due to electromigration in confined metal lines, J. Appl. Phys. **73** (1993) 3790-3799.

[4] Christiansen C, Li B, et al., Electromigration-resistance enhancement with CoWP or CuMn for advanced Cu interconnects, IEEE International Reliability Physics Symposium (Monterey, CA, 2011), p. 3E. 3.1.

[5] Vaidya S and Sinha AK, Effect of texture and grain structure on electromigration in Al-0.5%Cu thin films, Thin Solid Films **75**, 1981, 253-259.

[6] Galand R, Arnaud L,. Petitprez E, Brunetti G, Clement L, Waltz P and Wouters Y, Grain boundary as relevant microstructure feature for electromigration in advanced technology studied by Electron BackScattered Diffraction, International Interconnect Technology Conference Materials for Advanced Metallization (IITC/MAM), 2011.

[7] Budiman, AS, Besser PR, Hau-riege CS, Marathe A, Joo Y, Tamura N, Patel JR and Nix WD, Electromigration-Induced Plasticity: Texture Correlation and Implications for Reliability Assessment, J. Elec Mat, **38**, 2009, 379-391.

[8] Choi Z-S, Mönig R, Thompson CV and Burns M, Kinetics of Void Drift in Copper Interconnects MRS Symp. **914**, 2006, F08-03.

[9] Choi Z-S, Mönig R and Thompson CV, Activation energy and prefactor for surface electromigration and void drift Cu interconnects J. Appl. Phys. **102**, 2007, 083509.

[10] Dwyer VM, An investigation of Electromigration induced void nucleation time statistics in short copper interconnects. J. Appl. Phys, 107 (2010) 103718.

[11] Hauschildt M, Gall M, Thrasher S, Justison P, Michaelson L, Hernandez R, Kawasaki H.and Ho PS,.Statistical Analysis of Electromigration Lifetimes and Void Evolution, 7th International Workshop on Stress-Induced Phenomena in Metallization. AIP Conference Proceedings, Volume 741, pp. 112-123 (2004).

[12] Dwyer VM, An analytical model of the microstructure in near-bamboo interconnects, J. Phys. D: Appl. Phys. **37** (2004) 422– 431.

[13] Choi, Z-S, Lee J, Lim MK, Gan CL, and Thompson CV, Void dynamics in copper-based interconnects J. Appl. Phys. **110**, 2011, 033505.

[14] Dwyer VM, Modeling the electromigration failure time distribution in short copper interconnects. J. Appl. Phys, 104 (2008) 053708.

[15] Lin MH, Lin MT and Wang T, Effects of length scaling on Electromigration in dual damascene copper interconnects. Microelectr. Reliab. 2008;48:569–77.

[16] Lim MK, Gan CL, Tan TL, Ee YC. Ng, CM, Zhang BC and Tan JB, Effects of pulsed current on electromigration lifetime, 15th International Symposium on the Physical and Failure Analysis of Integrated Circuits, IPFA 2008.

[17] Doyen L, Arnaud L, Federspiel X, Waltz P and Wouters Y, Use of bidirectional current stress for in depth analysis of Electromigration mechanism, IEEE International Reliability Physics Symposium (Pheonix, AZ, 2008). 681–682.